THE JOURNAL OF NAVIGATION (2021), **74**, 143–155.
doi:10.1017/S0373463320000405

A New Method of Real-Time Kinematic Positioning Suitable for Baselines of Different Lengths

Jinhai Liu[1,2], Rui Tu[1,2,3], Rui Zhang[1,3], Xiaodong Huang[1,2], Pengfei Zhang[1,2] and Xiaochun Lu[1,2,3]

[1](*National Time Service Center, Chinese Academy of Sciences, Xi'an, China*)
[2](*University of Chinese Academy of Sciences, Beijing, China*)
[3](*Key Laboratory of Time and Frequency Primary Standards, Chinese Academy of Sciences, Xi'an, China*)
(E-mail: turui-2004@126.com)

This study introduces a new real-time kinematic (RTK) positioning method which is suitable for baselines of different lengths. The method merges carrier-phase wide-lane, and ionosphere-free observation combinations (LWLC) instead of using pseudo-range, and carrier-phase ionosphere-free combination (PCLC), or single-frequency pseudo-range and phase combination (P1L1). In a first step, the double-differenced wide-lane ambiguities were calculated and fixed using the pseudo-range and carrier-phase wide-lane combination observations. Once the double-differenced wide-lane integer ambiguities were known, the wide-lane combined observations were regarded as accurate pseudo-range observations. Subsequently, the carrier-phase wide-lane, and ionosphere-free combined observations were used to fix the double-differenced carrier-phase integer ambiguities, achieving the final RTK positioning. The RTK positioning analysis was performed for short, medium, and long baselines, using the P1L1, PCLC, and LWLC methods, respectively. For a short baseline, the LWLC method demonstrated positioning accuracy similar to the P1L1 method, and performed better than the PCLC method. For medium and long baselines, the positioning accuracy of the LWLC method was slightly higher than those of the PCLC and P1L1 methods. In conclusion, the LWLC method provided high-precision RTK positioning results for baselines with different lengths, as it used high-precision carrier-phase observations with fixed ambiguities instead of low-precision pseudo-range observations.

KEYWORDS

1. Global Navigation Satellite System. 2. Real-Time Kinematic. 3. Baseline. 4. Ambiguity Resolution. 5. Accuracy. 6. Reliability.

Submitted: 1 March 2019. Accepted: 11 July 2020. First published online: 11 August 2020.

1. INTRODUCTION. Real-time kinematic (RTK) is a technique to enhance the precise positioning of global navigation satellite systems (GNSS). As users can obtain centimetre-level positioning results in real time, it is widely applied in many high-precision

engineering fields like control measurements and deformation monitoring (Dai et al., 2007; Tang et al., 2014; He et al., 2016; Gao et al., 2017).

The reliable work range of RTK lies generally within a few kilometres. As the spatial correlation decreases with the increase of the distance between reference and rover stations, it is difficult to fix the carrier-phase integer ambiguity accurately by a simple combination of double-differences for a long baseline, resulting in a deterioration of the positioning performance (He et al., 2014; Odolinski et al., 2015a; Paziewski and Sieradzki, 2017). Traditional data solution methods for RTK include: single-frequency pseudo-range and carrier-phase combined observations (P1L1) and pseudo-range and carrier-phase ionosphere-free combined observations (PCLC). The method of P1L1 is simple and does not amplify the measurement noise; however, the single-frequency observations cannot eliminate the effects of the ionospheric error. With a short baseline, the double-differenced method can efficiently reduce the influence of the ionospheric error, and the P1L1 method can obtain positioning results at centimetre level. However, as the baseline length increases, spatially related error terms need to be considered. The ionosphere-free combined observations of the PCLC method can eliminate the effects of ionospheric delay, but pseudo-range observations have a low accuracy, and ionosphere-free combined observations amplify the measurement noise, and require a longer initialisation to isolate the carrier ambiguity parameters precisely to obtain positioning results at centimetre level. Both of these data solution methods have their own merits, but they also have obvious limitations.

A variety of studies have been carried out to enhance RTK techniques. Odolinski et al. (2015b) studied the combined single-frequency or dual-frequency single baseline model (GPS-BDS) RTK, using different data solution methods for different baselines lengths. They applied the ionospheric fixed model for short baselines, the ionospheric weighted model for medium baselines, and the ionospheric float model for long baselines. For parameter estimations, they used the single epoch solution for short and medium baselines, and the Kalman filtering estimation for long baselines. Under conditions of a 25° cut-off elevation angle, the combined system showed that the ambiguity float solution reached faster convergence; with a quicker and more accurate ambiguity resolution, fast and high-precision positioning was achieved. Tu et al. (2019) introduced the BeiDou navigation satellite system (BDS) zero-combined RTK algorithm by adding the ionospheric constraints to correct accurately the double-differenced ionospheric residuals. The positioning bias, after applying the double-frequency ionospheric constraints, was more stable than that of the ionosphere-free combination; the positioning accuracy of BDS RTK reached 1–2 cm for the long baseline of about 100 km. Brack (2017) analysed the impact of partial ambiguity resolution (PAR) techniques on the positioning performance of dual-frequency single and combined GPS and BDS RTK for long baselines. Compared with the conventional full ambiguity resolution (FAR) schemes, the experimental results demonstrated that the time taken to reach centimetre-level positioning results was significantly reduced when using PAR techniques, especially for the combined system. It was also shown that it was often not required to resolve the full set of ambiguities to achieve close to optimal positioning accuracy.

The above methods offer a number of advancements to improve the performance of the RTK. Finding a simple RTK method for baselines of different lengths which offers powerful operability and achieves good positioning results is a worthwhile endeavour. Therefore, this study presents a new RTK positioning method which is suitable for baselines of different lengths. In a first step, the double-differenced wide-lane ambiguities were estimated and

https://doi.org/10.1017/S0373463320000405 Published online by Cambridge University Press

fixed using the pseudo-range and carrier-phase wide-lane combined observations. Once the double-differenced wide-lane integer ambiguities were known, the wide-lane combined observations were regarded as high-precision pseudo-range observations. Subsequently, the carrier-phase wide-lane and ionosphere-free combined observations were used to fix the double-differenced carrier-phase integer ambiguities, achieving the final RTK positioning.

Based on the introduction of the conventional RTK model, this study proposes a new RTK positioning method which is suitable for baselines of different lengths. Assessments and discussions are provided regarding the feasibility of this approach.

2. METHODS.

2.1. *Mathematic model.* RTK positioning often uses the double-differenced observation model, which not only eliminates the satellite clock and receiver clock error, but also significantly softens the influence of errors like ionospheric and tropospheric delays, satellite orbit, and others (He et al., 2014; Li et al., 2017; Tu et al., 2018). In this study, the effects of the ionospheric and tropospheric residuals are ignored, and only the coordinates and double-differenced ambiguity parameters are estimated.

2.1.1. *Single-frequency pseudo-range and carrier-phase combination (P1L1).* Double-differenced pseudo-range and carrier-phase L1 observation equations respectively, can be expressed as:

$$\nabla\Delta P_{1,AB}^{ij} = \nabla\Delta\rho_{AB}^{ij} + \nabla\Delta I_{AB}^{ij} + \nabla\overline{M}_{W,AB}^{ij}\overline{T}_{W,AB} + \nabla\Delta e_{1,AB}^{ij} \tag{1}$$

$$\lambda_1\nabla\Delta\phi_{1,AB}^{ij} = \nabla\Delta\rho_{AB}^{ij} + \lambda_1\nabla\Delta N_{1,AB}^{ij} - \nabla\Delta I_{AB}^{ij} + \nabla\overline{M}_{W,AB}^{ij}\overline{T}_{W,AB} + \nabla\Delta\varepsilon_{1,AB}^{ij} \tag{2}$$

where $\nabla\Delta(\cdot)$ is the double-differenced operator; P and ϕ are pseudo-range and carrier-phase observations, respectively; superscript i and j represent different satellites; subscript 1 represents the frequency; subscripts A and B represent different stations; ρ is the distance between the station and the satellite; I is the first-order term of the ionospheric delay error; $\nabla\overline{M}_{W,AB}^{ij}$ is the average of wet delay projection coefficients for the single-difference tropospheric delay between two stations; $\overline{T}_{W,AB}$ is the average zenith tropospheric wet delay between two stations; λ_1 is the narrow lane wavelength; $\boldsymbol{N}$ is the ambiguity vector; $\boldsymbol{e}$, $\boldsymbol{\varepsilon}$ are the measurement noises of pseudo-range and carrier-phase observations, respectively.

2.1.2. *Pseudo-range and carrier-phase ionosphere-free combination (PCLC).* The double-differenced pseudo-range and carrier-phase ionosphere-free combined observation equations, respectively, can be expressed as:

$$\nabla\Delta P_{\mathrm{IF},AB}^{ij} = \nabla\Delta\rho_{AB}^{ij} + \nabla\overline{M}_{W,AB}^{ij}\overline{T}_{W,AB} + \nabla\Delta\varepsilon_{\mathrm{IF},AB}^{ij} \tag{3}$$

$$\begin{aligned}\lambda_{\mathrm{IF}}\nabla\Delta\varphi_{\mathrm{IF},AB}^{ij} &= \nabla\Delta\rho_{AB}^{ij} + \lambda_{\mathrm{IF}}\nabla\Delta N_{\mathrm{IF},AB}^{ij} + \nabla\overline{M}_{W,AB}^{ij}\overline{T}_{W,AB} + \nabla\Delta\varepsilon_{\mathrm{IF},AB}^{ij} \\ &= \nabla\Delta\rho_{AB}^{ij} + \lambda_{\mathrm{IF}}\left(\nabla\Delta N_{1,AB}^{ij} + \frac{f_2}{f_1 - f_2}\nabla\Delta N_{W,AB}^{ij}\right) + \nabla\overline{M}_{W,AB}^{ij}\overline{T}_{W,AB} + \nabla\Delta\varepsilon_{\mathrm{IF},AB}^{ij}\end{aligned} \tag{4}$$

where the subscript IF indicates the ionosphere-free combination; the $\nabla\Delta N_{IF}$ is the double-differenced ionosphere-free ambiguity, which is divided into the expression of the double-differenced L1 ambiguity, and the wide-lane ambiguity. When the wide-lane ambiguity is fixed, the carrier-phase L1 float ambiguity can be retrieved; the LAMBDA algorithm is

https://doi.org/10.1017/S0373463320000405 Published online by Cambridge University Press

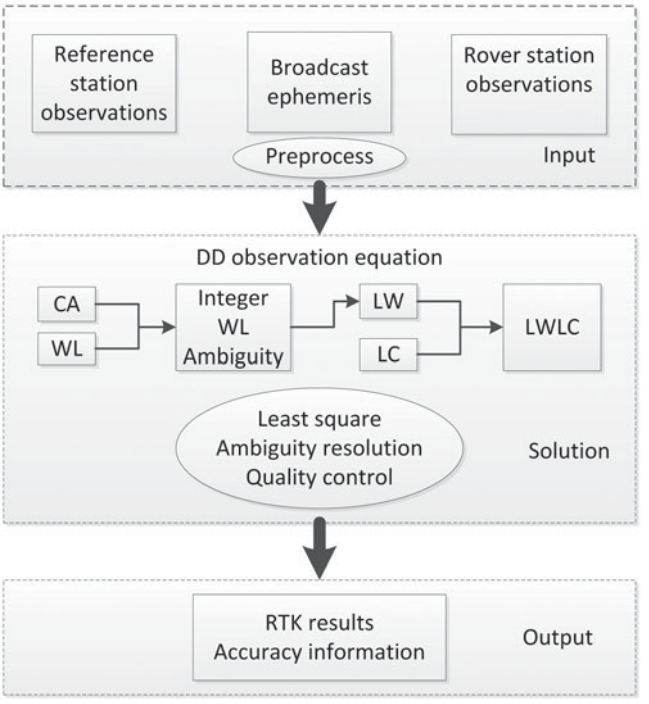

Figure 1. Flowchart of the LWLC data solution (CA = double-differenced pseudo-range observation equation; WL = double-differenced wide-lane combined observation equation; LW = wide-lane combined observation equation with double-differenced wide-lane ambiguity fixed; LC = phase ionosphere-free combined observation equation).

used to search for the L1 integer ambiguity, and the ratio value is used for verification to obtain the positioning results (Teunissen, 1995; Teunissen and Verhagen, 2009).

2.1.3. *Wide-lane phase and carrier-phase ionosphere-free combined observations (LWLC).* The double-differenced wide-lane combined observation equation can be expressed as Equation (5). The float solution of the wide-lane ambiguity is obtained by the sequential least squares adjustment method combined with the double-differenced pseudo-range observation Equation (1), subsequently searched and fixed by the LAMBDA algorithm.

$$\lambda_W \nabla \Delta \varphi^{ij}_{W,AB} = \nabla \Delta \rho^{ij}_{AB} + \lambda_W \nabla \Delta N^{ij}_{W,AB} + \frac{f_1}{f_2} \nabla \Delta I^{ij}_{AB} + \nabla \overline{M}^{ij}_{W,AB} \overline{T}_{W,AB} + \nabla \Delta \varepsilon^{ij}_{W,AB} \quad (5)$$

The double-differenced wide-lane combined observation equation with fixed double-differenced wide-lane ambiguity is the same as in Equation (5). In this case, the double-differenced wide-lane integer ambiguity is directly inserted into the equation as a known value, and merged with the phase ionosphere-free combined observation Equation (4) to solve the L1 double-differenced ambiguity and perform the positioning solution.

Figure 1 shows the flow chart of the LWLC method, which can be divided into three parts. The first part is the data input, using real-time reception observation data from reference and rover station, broadcast ephemeris, and preprocessing for a clean dataset.

https://doi.org/10.1017/S0373463320000405 Published online by Cambridge University Press

Table 1. Weight ratios between observations for different methods by GPS system.

Method	LWLC		PCLC		P1L1	
Observation	LW	LC	PC	LC	P1	L1
Weight ratio	100*c*20·5	10,000*c*3	1*c*3	10,000*c*3	1*c	10,000*c

Note: c = the weight matrix determined by the elevation angle.

The second part is the RTK estimation, using different observation combined models to constitute the double-differenced observation equation. The double-differenced wide-lane integer ambiguity uses the double-differenced pseudo-range observation equation, and the phase wide-lane combined observation equation by the sequential least adjustment method to obtain the float solution. Subsequently, the LAMBDA algorithm is used to search the wide-lane ambiguity, and the ratio value is used as a test (Teunissen, 1995; Teunissen and Verhagen, 2009), to obtain the integer WL ambiguity. After fixing the double-differenced wide-lane ambiguity, the double-differenced wide-lane combined observation equation is equivalent to a high-precision double-differenced pseudo-range observation equation; the observation residual is one order of magnitude smaller than the pseudo-range ionosphere-free combination. The carrier-phase ionosphere-free combined observation Equation (4) is used to solve the L1 float ambiguity, which is also searched by the LAMBDA algorithm and tested by the ratio values (Teunissen, 1995; Teunissen and Verhagen, 2009). The third part is the result output, using real-time output RTK positioning results, and accuracy information.

2.2. *Stochastic model.* Differences of measurement noise can be measured by the weight of the observation value. At the same time, the rationality and reliability of the observation weight matrix directly relate to the initialisation time of the ambiguity, the reliability of the ambiguity search, and the success rate. In this study, the elevation angle is used to determine the weights of the double-differenced observations. For epoch i, the constructed covariance matrix of the elevation angles can be written as follows (Gao et al., 2005):

$$D_i = \begin{bmatrix} 1+\dfrac{\sin E_1}{\sin E_r} & 1 & \cdots & 1 \\ 1 & 1+\dfrac{\sin E_2}{\sin E_r} & \cdots & 1 \\ \vdots & \vdots & \cdots & \vdots \\ 1 & 1 & \cdots & 1+\dfrac{\sin E_{n-1}}{\sin E_r} \end{bmatrix} \tag{6}$$

where E_r is the average of the elevation angles of the reference satellite of the two stations, $E_1, \cdots, E_{n-1}$ are the average of the elevation of the other n–1 common satellites of the two stations.

For the three methods of LWLC, PCLC, and P1L1, the weight ratios of different types of observations are set according to the noise characteristics of the observations, and the relationship between combined observations for the GPS system, shown in Table 1.

2.3. *Parameter estimation strategy.* As the ionospheric residuals and tropospheric residuals are ignored, there are only coordinate and ambiguity parameters for these three

https://doi.org/10.1017/S0373463320000405 Published online by Cambridge University Press

Table 2. Baselines and receiver types.

No.	Baseline	Length (km)	Date	Receiver antenna 1	Receiver antenna 2
1	STR1-TID1	9·7	DOY 125, 2017	SEPT POLARX5	SEPT POLARX5
2	HKSL-HKWS	42·5	DOY 074, 2018	LEICA GR50	LEICA GR50
3	NNOR-PERT	88·5	DOY 077, 2018	SEPT POLARX4	TRIMBLE NETR9

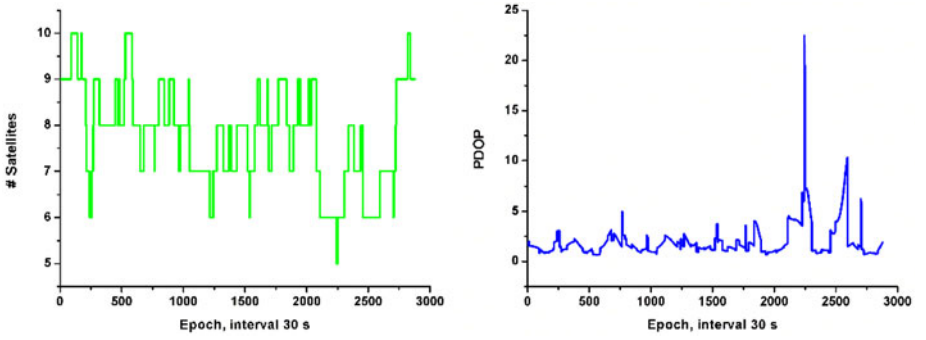

Figure 2. Baseline STR1-TID1 GPS satellites (left) and PDOP values (right).

methods. The least squares adjustment or Kalman filter method can be used for the parameter estimation. The dynamic noises of coordinate components for each epoch are set as zero and 5 m for the static and dynamic modes, respectively. The dynamic noise of the ambiguity is set as zero in each continuous arc, and it should be reinitialised when a cycle slip is detected.

3. VERIFICATION AND ANALYSIS.

3.1. *Dataset.* The test data is provided by the International GNSS Service (IGS) centre. The sampling interval is 30 s. The broadcast ephemeris is used. The precise coordinates of the stations are provided by the IGS's weekly solutions. The baseline information is shown in Table 2.

3.2. *Satellite number and PDOP value.* Figures 2–4 show the number of GPS satellites and position dilution of precision (PDOP) values corresponding to the baselines STR1-TID1, HKSL-HKWS, and NNOR-PERT. The average number of satellites is 7·8, 7·7, and 7·2; the average PDOP values are 1·9, 3·3, and 3·6, respectively.

3.3. *Residuals of pseudo-range observations.* Figure 5 shows the time series of double-differenced residuals of pseudo-range observations for three different methods of baselines STR1-TID1, HKSL-HKWS, and NNOR-PERT. Table 3 shows the statistics of residual standard deviation (STD) for pseudo-range observations for different methods and different baselines. In Figure 5 and Table 3 it can be seen that for different baseline lengths the residuals, when using wide-lane combined observations instead of pseudo-range observations, are smallest in the LWLC method; the PCLC method amplifies the pseudo-range measurement noises, exceeding those of the P1L1 method by approximately three times. Therefore, the use of wide-lane combined observations instead of pseudo-range observations is more advantageous in solving carrier-phase ambiguity parameters.

https://doi.org/10.1017/S0373463320000405 Published online by Cambridge University Press

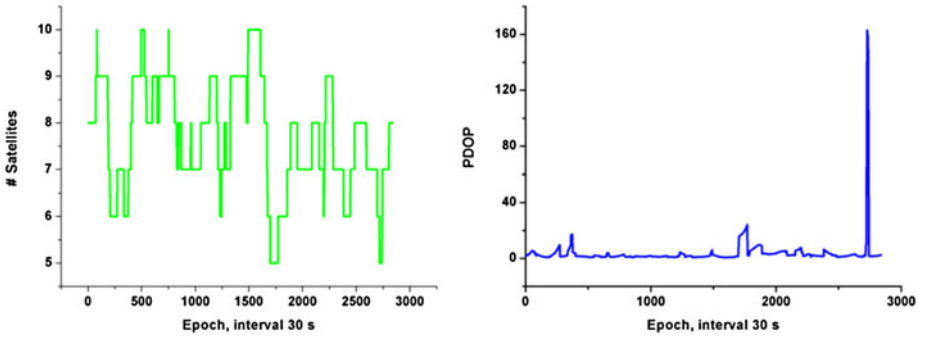

Figure 3. Baseline HKSL-HKWS GPS satellites (left) and PDOP values (right).

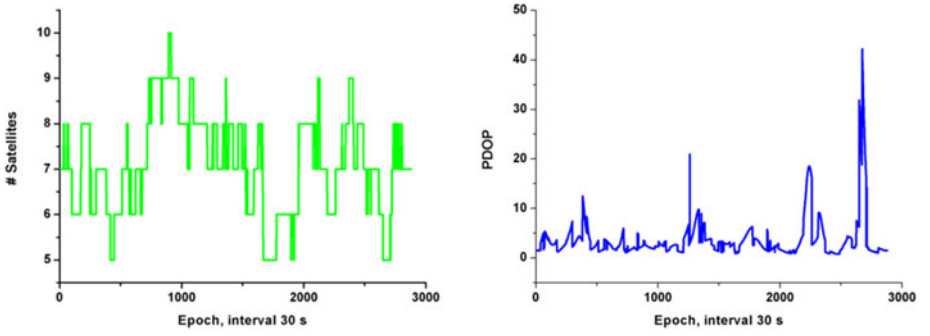

Figure 4. Baseline NNOR-PERT GPS satellites (left) and PDOP values (right).

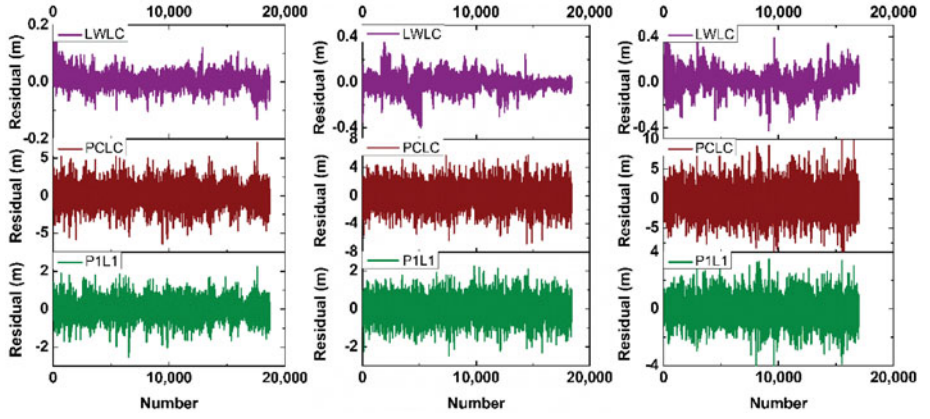

Figure 5. Time series of double-differenced residuals of pseudo-range observations for three different methods: STR1-TID1 (left), HKSL-HKWS (middle), NNOR-PERT (right).

3.4. *Residuals of carrier-phase observations.* Figure 6 shows the time series of double-differenced residuals of the carrier-phase observations for three different methods of baselines STR1-TID1, HKSL-HKWS, and NNOR-PERT. Table 4 shows the statistics of residual STD for the phase observations for different methods. In Figure 6, and

https://doi.org/10.1017/S0373463320000405 Published online by Cambridge University Press

Table 3. Statistics of STD of residuals for double-differenced pseudo-range observations for different methods and baselines.

	STD of residuals for pseudo-range observations (m)		
Baseline	LWLC	PCLC	P1L1
STR1-TID1	0·02444	0·98773	0·34607
HKSL-HKWS	0·07175	1·52854	0·55828
NNOR-PERT	0·08728	1·83409	0·66750

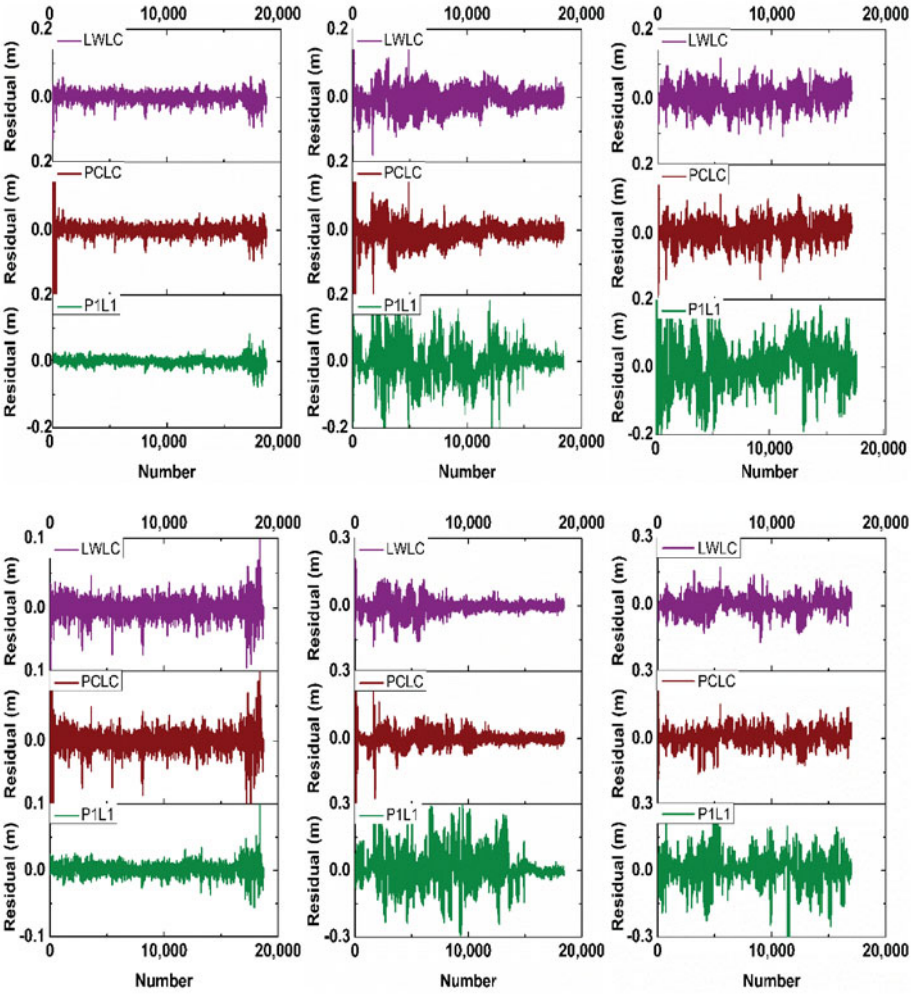

Figure 6. Time series of the double-differences residuals for carrier-phase observations for three different methods: STR1-TID1(left), HKSL-HKWS (middle), NNOR-PERT(right). (The three subgraphs above represent the static solution, and the three subgraphs below represent the simulated dynamic solution.)

https://doi.org/10.1017/S0373463320000405 Published online by Cambridge University Press

Table 4. Statistics of STD of residuals for the carrier-phase residuals for different methods and baselines.

Position mode	Baseline	STD of residuals for carrier-phase observations (cm)		
		LWLC	PCLC	P1L1
Static	STR1-TID1	0·832	0·833	0·665
	HKSL-HKWS	1·223	1·241	3·289
	NNOR-PERT	2·654	2·572	3·227
Simulated kinematic	STR1-TID1	1·036	3·321	0·778
	HKSL-HKWS	2·977	3·681	7·048
	NNOR-PERT	3·292	3·283	6·297

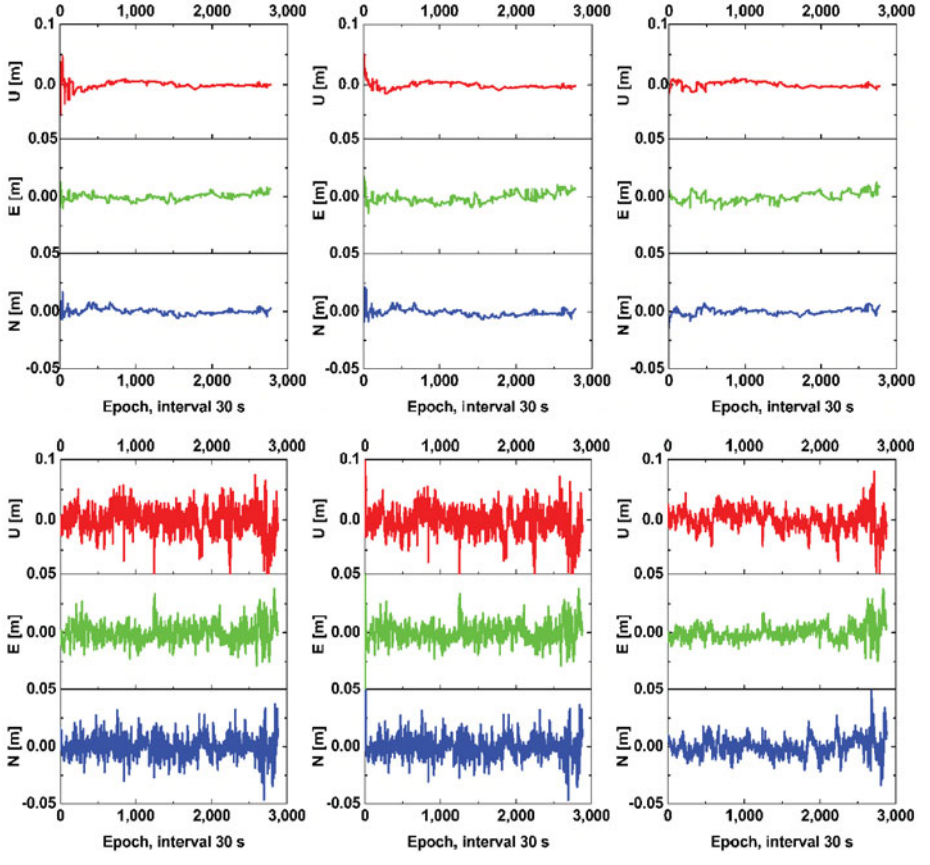

Figure 7. Positioning bias for three different methods of baseline STR1-TID1: LWLC (left), PCLC (middle), P1L1 (right). (The three subgraphs above represent the static solution, and the three subgraphs below represent the simulated kinematic solution.)

https://doi.org/10.1017/S0373463320000405 Published online by Cambridge University Press

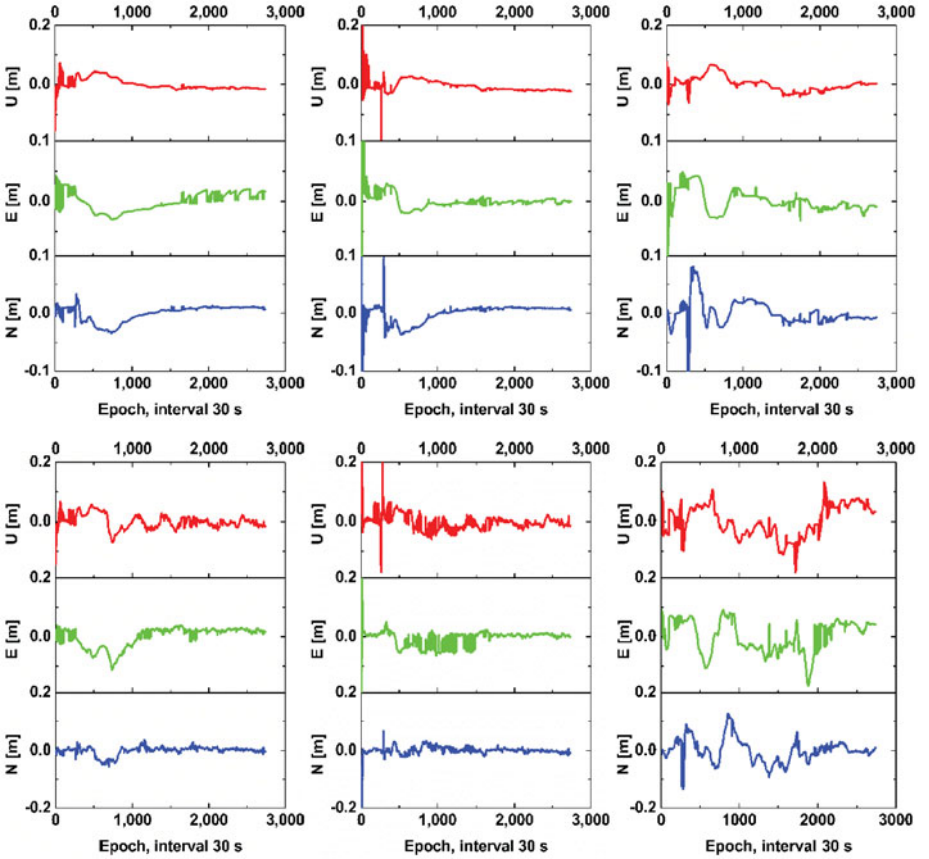

Figure 8. Positioning bias for three different methods of baseline HKSL-HKWS: LWLC (left), PCLC (middle), P1L1 (right). (The three subgraphs above represent the static solution, and the three subgraphs below represent the simulated kinematic solution.)

Table 4, for baseline STR1-TID1, residuals of the carrier-phase observations in the P1L1 method are the smallest, while residuals using the LWLC and PCLC methods are equivalent, because the combined observations amplify the measurement noise. With shorter baselines, the residuals like ionospheric and tropospheric delays are relatively small, and the ambiguity is relatively easy to fix. For baselines HKSL-HKWS, and NNOR-PERT, the ionospheric residuals are relatively large in the P1L1 method, and the measurement noise of the carrier-phase observations in the P1L1 method is stronger than in LWLC and PCLC.

3.5. *The bias of positioning.* Figures 7–9 show the bias of positioning corresponding to the static and simulated kinematic solutions for three different methods of baselines STR1-TID1, HKSL-HKWS, and NNOR-PERT, respectively. For the short baseline, the bias of positioning levels for three different methods, shown in Figure 7, are comparable; the PCLC method has a slightly larger deviation during the initialisation stage, whereas the LWLC and P1L1 methods have a smaller deviation during the initialisation stage. For the medium and long baselines, differences of the positioning error in the three different methods, shown in Figures 8 and 9, are slightly larger. Especially during the initialisation stage, the LWLC method is optimal. Table 5 provides the statistics of the positioning accuracy

https://doi.org/10.1017/S0373463320000405 Published online by Cambridge University Press

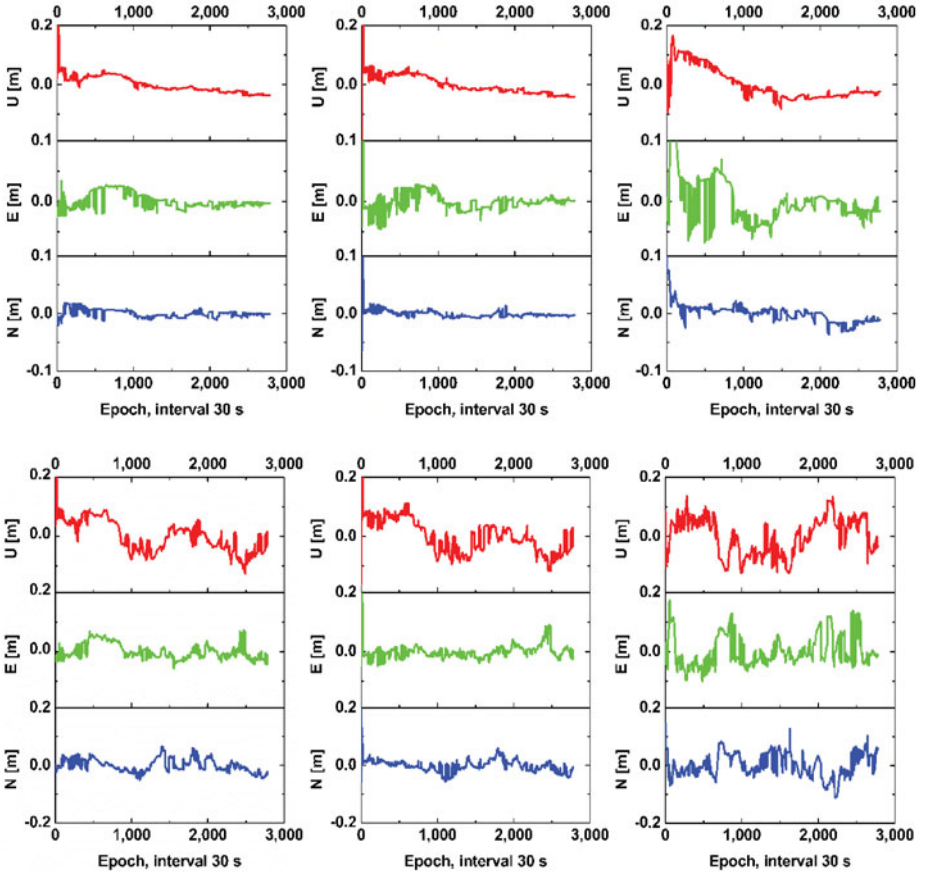

Figure 9. Positioning bias for three different methods of baseline NNOR-PERT: LWLC (left), PCLC (middle), P1L1 (right). (The three subgraphs above represent the static solution, and the three subgraphs below represent the simulated kinematic solution.)

for different baselines and different methods. It can be seen in Table 5 that the residuals of ionospheric and tropospheric delay errors are negligible for a short baseline. The LWLC and the P1L1 method have the same positioning accuracy in the north (N), east (E), and up (U) components, which is better than 1 cm in the N and E components and better than 2 cm in the U components; the PCLC method delivers relatively poor positioning results. For the medium and long baselines, the positioning accuracy of the LWLC method is higher than that of the PCLC and P1L1 methods. The LWLC method delivers high-precision RTK positioning for short, medium, and long baselines, and greater stability regarding positioning deviations. In addition, from Figure 7, it can be seen that there are also large differences in the noises of the positioning biases; the P1L1 method is the smallest, and the LWLC method is a little larger than the P1L1 method. The PCLC method is the largest for the short baseline, and these results are also consistent with the former discussions. In Figures 7 and 8, the positioning biases with some spikes for the PCLC and P1L1 methods can be observed; these are mainly caused by the failure of the ambiguity resolution, and the results of the LWLC method are satisfactory.

https://doi.org/10.1017/S0373463320000405 Published online by Cambridge University Press

Table 5. Positioning accuracy for different baselines and different methods.

		STD of positioning error(cm)								
		LWLC			PCLC			P1L1		
Position mode	Baseline	*N*	*E*	*U*	*N*	*E*	*U*	*N*	*E*	*U*
Static	STR1-TID1	0·253	0·275	0·519	1·128	1·159	1·890	0·248	0·391	0·471
	HKSL-HKWS	1·368	1·566	1·975	2·503	2·841	3·698	2·266	1·988	2·531
	NNOR-PERT	0·634	1·247	2·877	2·144	2·177	3·507	1·555	4·117	5·391
Simulated kinematic	STR1-TID1	0·815	0·764	1·894	2·117	2·877	3·596	0·760	0·655	1·697
	HKSL-HKWS	1·403	3·448	2·335	2·184	3·102	4·007	4·023	5·488	5·378
	NNOR-PERT	2·210	2·669	5·328	2·757	2·646	5·848	4·020	5·195	6·335

4. CONCLUSION AND DISCUSSION. A new RTK positioning method is proposed which is suitable for baselines of different lengths. The method uses a combination of wide-lane combined observations and carrier-phase ionosphere-free observations instead of pseudo-range and carrier-phase ionosphere-free combinations or single-frequency pseudo-range and carrier-phase combinations. The wide-lane combined observations with known integer wide-lane ambiguities are regarded as high-precision pseudo-range observations which enhance the separation of L1 ambiguity parameters from position parameters, and achieve a rapid positioning with an accuracy at centimetre level. The final positioning result is the response of observation noise, observation precision, and ionosphere residuals. Compared with the P1L1 method, the LWLC method not only demonstrated higher precision code observation, but also lacked ionospheric residuals. Compared with the PCLC method, the LWLC method not only demonstrated higher precision code observation, but also smaller observation noise, thus it is suitable for different baselines. The analysis of the positioning results based on short, medium, and long baseline observations verifies the feasibility and effectiveness of the method. The main conclusions are as follows:

1. For short baselines, the LWLC and P1L1 methods have the same positioning accuracy in the N, E, and U components. The N and E components are better than 1 cm, and the U component is better than 2 cm. The PCLC method delivers relatively poor positioning results.
2. For medium and long baselines, the positioning accuracy of the LWLC method is higher than that of the PCLC and P1L1 methods.
3. For the LWLC method, the residual of STD of the virtual pseudo-range observations is replaced by phase observations with fixed double-differenced wide-lane ambiguities at the centimetre level; they are two orders of magnitude higher than for the PCLC and P1L1 methods.

This paper analyses only the data of a single GPS system for feasibility purposes. Multi-GNSS and multi-frequency data are needed to improve and verify accuracy and reliability, especially for dynamic observation data.

In addition, the double-differenced P1 and wide-lane observations were directly used to solve the ambiguity of wide lane by sequential least squares adjustment method. As the double-differenced observation was used and the wide-lane ambiguity also with long wavelength, this study did not consider the residuals of ionospheric and tropospheric delay for the estimation of wide-lane ambiguity. Finally, while for the medium or long baselines the

https://doi.org/10.1017/S0373463320000405 Published online by Cambridge University Press

effects of ionospheric and tropospheric residuals may influence the parameter solution, thus, in this case, the ionospheric and tropospheric residuals can also be estimated as unknown parameters (Gao et al., 2017; Tu et al., 2019). This also needs to be further studied in the future.

ACKNOWLEDGEMENTS

This work was partly supported by the National Natural Science Foundation of China (Grant No: 41504006, 41674034, 41704008), National Key Research and Development Plan of China (Grant No: 2016YFB0501804), Chinese Academy of Science (CAS) programs of 'Pioneer Hundred Talents' (Grant No: Y923YC1701) and 'Key Research Program of Frontier Sciences' (Grant No: QYZDB-SSW-DQC028).

REFERENCES

Brack, A. (2017). Long Baseline GPS + BDS RTK Positioning with Partial Ambiguity Resolution. *Proceedings of the 2017 International Technical Meeting of The Institute of Navigation*, Monterey, California, January 2017, pp. 754–762.

Dai, L., Eslinger, D. and Sharpe, T. (2007). Innovative Algorithms to Improve Long Range RTK Reliability and Availability. *Proceedings of the National Technical Meeting of the Institute of Navigation NTM*, Vol. 6682(1), pp. 860–872.

Gao, C., Zhao, Y. and Wan, D. (2005). The weight determination of the double difference observation in GPS carrier phase positioning. *Science of Surveying and Mapping*, **30**(3), 28–32.

Gao, W., Gao, C., Pan, S., Meng, X. and Xia, Y. (2017). Inter-system differencing between GPS and BDS for medium-baseline RTK positioning. *Remote Sensing*, **9**(9), 948–964. doi:10.3390/rs9090948

He, H., Li, J., Yang, Y., Xu, J., Guo, H. and Wang, A. (2014). Performance assessment of single- and dual-frequency BeiDou/GPS single-epoch kinematic positioning. *GPS Solutions*, **18**(3), 393–403. doi:10.1007/s10291-013-0339-3

He, X., Zhang, X., Tang, L. and Liu, W. (2016). Instantaneous real-time kinematic decimeter-level positioning with BeiDou triple-frequency signals over medium baselines. *Sensors*, **16**(1), 1. doi:10.3390/s16010001

Li, G., Wu, J., Zhao, C. and Tian, Y. (2017). Double differencing within GNSS constellations. *GPS Solutions*, **21**(3), 1161–1177. doi:10.1007/s10291-017-0599-4

Odolinski, R., Teunissen, P. J. G. and Odijk, D. (2015a). Combined BDS, Galileo, QZSS and GPS single-frequency RTK. *GPS Solutions*, **19**(1), 151–163. doi:10.1007/s10291-014-0376-6

Odolinski, R., Teunissen, P. J. G. and Odijk, D. (2015b). Combined GPS + BDS for short to long baseline RTK positioning. *Measurement Science and Technology*, **26**(4), 045801. doi:10.1088/0957-0233/26/4/045801

Paziewski, J. and Sieradzki, R. (2017). Integrated GPS + BDS instantaneous medium baseline RTK positioning: signal analysis, methodology and performance assessment. *Advances in Space Research*, **60**(12), 2561–2573. doi:10.1016/j.asr.2017.04.016

Tang, W., Jin, L. and Xu, K. (2014). Performance analysis of ionosphere monitoring with BeiDou CORS observational data. *Journal of Navigation*, **67**(1), 511–522. doi:10.1017/S0373463313000854

Teunissen, P. J. G. (1995). The least-squares ambiguity decorrelation adjustment: a method for fast GPS integer ambiguity estimation. *Journal of Geodesy*, **70**(1), 65–82. doi:10.1007/BF00863419

Teunissen, P. J. G. and Verhagen, S. (2009). The GNSS ambiguity ratio-test revisited: a better way of using it. *Survey Review*, **41**(312), 138–151. doi:10.1179/003962609X390058

Tu, R., Liu, J., Zhang, R., Zhang, P. and Lu, X. (2018). A model for combined GPS and BDS real-time kinematic positioning using one common reference ambiguity. *Journal of Navigation*, **71**(4), 1011–1024. doi:10.1017/S0373463318000061

Tu, R., Lu, C., Zhang, P., Zhang, R., Liu, J. and Lu, X. (2019). The study of BDS RTK algorithm based on zero-combined observations and ionosphere constraints. *Advances in Space Research*, **63**(9), 2687–2695. doi:10.1016/j.asr.2017.07.023